THE ASTROPHYSICAL JOURNAL, 473:L17–L20, 1996 December 10

GALAXY DARK MATTER: GALAXY-GALAXY LENSING IN THE HUBBLE DEEP FIELD[1]

IAN P. DELL'ANTONIO AND J. ANTHONY TYSON
Bell Laboratories, Lucent Technologies, 700 Mountain Avenue, Murray Hill, NJ 07974; dellantonio@bell-labs.com, tyson@bell-labs.com
Received 1996 March 12; accepted 1996 September 27

ABSTRACT

In this Letter we present calibrated observations of the average mass of galaxies with $22 < I < 25$ in the Hubble Deep Field. We measure the mean mass profile using the statistical gravitational lens distortion of faint blue background galaxies, based on 2221 foreground-background pairs. The observed weak lensing distortion is calibrated via full three-dimensional simulations and other *Hubble Space Telescope* data on a foreground cluster of known mass.

Inside a projected radius of 5″ we find a 3 σ detection of shear. Fitting to an isothermal mass distribution, we find a distortion of $0.066^{+0.018}_{-0.019}$ at a radius of 2″ ($\sim 8\,h^{-1}$ kpc). The (1σ) limits on the parameters for the truncated isothermal model are $\sigma_v = 185^{+30}_{-35}$ km s^{-1}, $r_{\rm outer} \geq 15\,h^{-1}$ kpc, and $r_{\rm core} = 0.6^{+1.3}_{-0.6}\,h^{-1}$ kpc. This corresponds to an average galaxy mass interior to 20 h^{-1} kpc of $5.9^{+2.5}_{-2.7} \times 10^{11}\,h^{-1}\,M_\odot$. Inside 10 h^{-1} kpc, we find an average rest-frame V-band mass-to-light ratio of $11.4^{+6.0}_{-6.7}\,h\,(M/L_V)_\odot$.

Subject headings: dark matter — galaxies: fundamental parameters — gravitational lensing

1. INTRODUCTION

The mass in the dark halos around individual field galaxies has long been debated. While there are compelling kinematic data on our own galaxy (Fich & Tremaine 1991) and pairs of galaxies (Zaritsky & White 1994), suggesting halos with equivalent circular velocities of ~200 km s^{-1} extending as far as 30 kpc, direct measures of mass using weak gravitational lens distortions have been difficult. Typical galaxies produce ~1″ deflections, resulting in relatively small shear at radii greater than 5″. Strong lensing of background QSOs has provided a spot check of total enclosed mass in several cases (Kochanek 1991), confirming masses of $\sim 1 - 2 \times 10^{11}\,h^{-1}\,M_\odot$ within $4\,h^{-1}$ kpc. However, the known lensed QSOs may selectively sample the tail of the galaxy mass distribution (Wallington & Narayan 1993).

Statistical gravitational lens distortion in a large sample of galaxies can address the more general question of the mean mass of all galaxies. Previous attempts to measure the average total mass of a large sample of galaxies by statistical weak lensing were hampered by seeing and systematic error (Tyson et al. 1984, hereafter TVJM84; Tyson 1987). Studying weak shear at radii >5″ in a 4.′8 radius field taken with the Palomar 5 m telescope, Brainerd, Blandford, & Smail (1996) recently claimed evidence for massive halos extending beyond $30\,h^{-1}$ kpc. The Hubble deep field (HDF) data, being multiband, high spatial resolution, and very deep, despite the small size of the field, provide a large volume sample and an opportunity to control systematics and bring the mass signal at less than 5″ out of the noise.

Here we report a calibrated measurement of the mass profile of field galaxies in the HDF. Galaxies with the faint surface brightness and colors of the distant faint blue galaxy population are used as background galaxies. We examined 2221 foreground-background pairs of galaxies for the induced shear from the foreground galaxy. We compare our result for the HDF with full three-dimensional simulations, with deep *HST* weak lens studies around a cluster of galaxies and with broader but "shallower" *HST* surveys. A comprehensive description of the cluster *HST* WFPC2 weak lens shear efficiency calibrations and comparison with other galaxy-galaxy weak lensing observations using *HST* and ground-based imaging will be given elsewhere.

[1] Based on observations with the NASA/ESA *Hubble Space Telescope*, obtained at the Space Telescope Science Institute, which is operated by AURA, under NASA contract NAS 5-26555.

2. IMAGE PROCESSING AND PHOTOMETRY CATALOGS

For this study, we used the "drizzled" HDF version 2 data in which the dithered images were combined on a resampling scale of 0.04″ pixel^{-1}. The HDF observations and pipeline processing are described in Williams et al. (1996). These reconstructed images cover 4.3 arcmin^2 for all three WFPC2 chips. The sky noise on 1″ scales in these reconstructed images is 28 B mag arcsec^{-2} and 28.5 R mag arcsec^{-2}. For this analysis we limit ourselves to the three deepest bands: F814W, F606W, and F450W (hereafter called I, R, and B). We re-analyze the images using FOCAS to produce photometrically accurate matched catalogs. The zero-points in the various filter bands are set by the HDF calibration (Williams et al. 1996).

We calculate magnitudes and colors using an equal-isophote method: initial object lists are constructed by running FOCAS on $B + R + I$ master images. This produces a master list of objects and isophotal regions. Magnitudes are then computed from the individual filter images using these identical isophotal areas, so the color estimates are not biased by systematic variations of the isophotes from band to band. This procedure yields magnitudes and intensity-weighted moments measured accurately in three bands. At a limiting magnitude of 29 B mag, about 40 galaxies between 24 and 29 mag will lie within a 10″ circle projected on any foreground galaxy.

In order to extract the lensing distortion, we must reliably measure the ellipticity and orientation of a faint galaxy. The faint background galaxies we use are quite small: the profile of a typical 27th mag arclet is shown in Figure 1. Useful surface photometry of these faint blue galaxies in the HDF data is

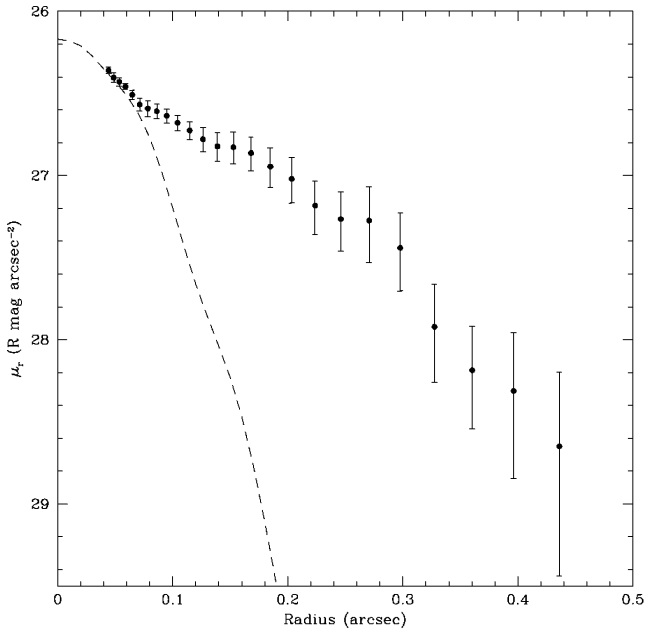

FIG. 1.—Surface brightness profile of a typical 27 mag arclet in the HDF. Accurate second moments for shear measurement require a limiting surface brightness of 28–29 mag arcsec^{-2} for these galaxies. Note that because the surface brightness is measured by averaging in elliptical annuli, adjacent annuli sample some of the same pixels, and hence the data points are correlated and the error bars only represent the photon statistics. The dashed line is the average *R*-band WFPC2 PSF.

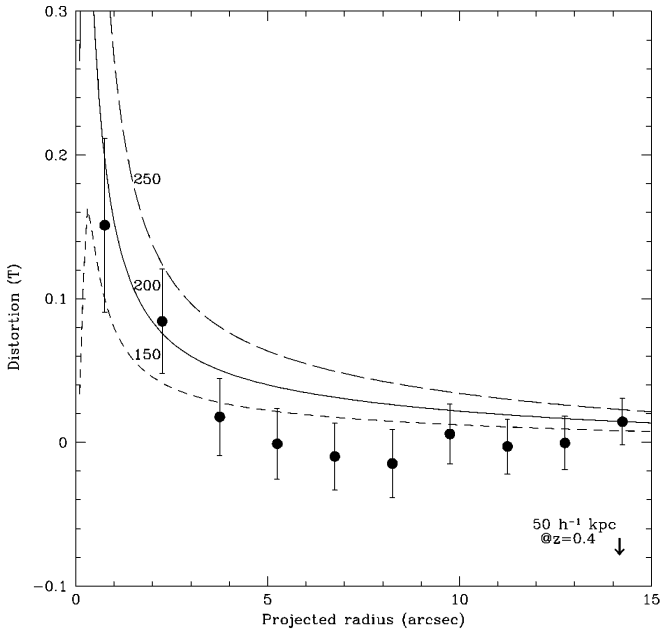

FIG. 2.—Observed distortion of the background galaxies, in 1.″5 independent bins, around the positions of foreground galaxies for 2221 foreground-background pair candidates in the three WFC fields of the HDF. The background/foreground selection was based on colors, surface brightness, and total magnitude difference. The lines show distortion from full three-dimensional calibrated simulations of truncated isothermal models with σ_v as labeled, $r_{\rm outer} = 30\,h^{-1}$ kpc, and $r_{\rm core} = 1\,h^{-1}$ kpc.

possible only within $r \sim 0.''5$. Simulations of random galaxy shapes using the observed noise characteristics of the HDF field show that we can measure ellipticity for galaxies as faint as 28 B mag and ellipticity 0.3 with an uncertainty in ellipticity less than 0.1. This suggests that we can safely use galaxies down to $B = 27.5$ as potential probes of the distortion.

3. ARCLET ANALYSIS AND MASS MODEL SIMULATIONS

To minimize the contamination from foreground galaxies, we use the color and apparent magnitude of the galaxies as rough statistical redshift estimators.

Any galaxy in the magnitude range $22 < I < 25$ (roughly redshift 0.2–0.7) is a candidate foreground lensing galaxy. Blue galaxies with $B - R < 0.3$ that are fainter than a candidate foreground galaxy but brighter than 27.5 *B* mag are candidate background galaxies. Because of competing volume and faint-end luminosity function effects, these faint galaxies cover a wide range in redshifts extending from $z = 1$–3; blue low surface brightness sources are likely to be at the highest redshifts. The trend toward redshift 1 at 25th mag is clear in a magnitude: log *z* plot (Koo & Kron 1992; Schade et al. 1995; Lilly et al. 1995).

Using this selection, we find 110 candidate lenses and 645 candidate background objects yielding 2221 candidate foreground-background pairs in the three WFPC2 CCD area of the HDF. We use FOCAS to calculate the intensity-weighted second moment in the *R* band for each source galaxy image (arclet) within 15″ of a candidate foreground galaxy. We calculate the x^2, y^2 and xy intensity moments (apodized with a Gaussian kernel of size equal to the half-light radius) transformed to (r, θ) moments relative to each foreground galaxy center (TVJM84; Tyson, Valdes, & Wenk 1990). These principal-axis transformed second moments of the arclets within some annulus about all candidate foreground galaxies are averaged together to give the observed distortion at that radius.

This observed distortion as a function of radius for all 2221 pairs is plotted in Figure 2. The points are the observed independent shear values in each radius bin, and the error bars obtained via the full simulations are consistent with bootstrap resampling errors. As always, the largest noise source is from the randomly oriented nonzero ellipticities of the source galaxies. We find a 3σ significance positive mass effect observed at radii less than a few arcseconds ($\sim 10\,h^{-1}$ kpc for $0.2 < z_{fg} < 0.7$). While we have not "tuned" the arclet color to maximize the distortion, if we relax the blue selection this distortion decreases; this is consistent with the blue $B - R$ colors of the highest redshift galaxies.

What galaxy mass distribution would generate this observed distortion? In selecting our sample galaxies based on brightness and color, the observed shear will be diluted by the convolution of the separate redshift distributions of the candidate lenses and arclets. The WFPC2 point spread function (PSF) and the drizzle algorithm have an effect on observed distortion for arclets whose surface brightness falls below about 28 mag arcsec^{-2} inside 0.2″ radius. Therefore, we must calibrate the lens mass which would generate this observed statistical distortion. We do this in two steps: (1) full three-dimensional simulations of the HDF, and then (2) comparison of a similar three-dimensional simulation with the weak lensing distortion of this signal same faint blue galaxy population observed with *HST* WFPC2 around a cluster of galaxies of known redshift and mass.

3.1. *Mass Calibration*

We calibrate the shear-mass relationship by simulating galaxy-galaxy lens distortions including multiple scattering effects. Realistic simulated field galaxies consistent with mild luminosity evolution (Im et al. 1995) are randomly distributed in seven redshift shells. These simulated galaxies have the same properties as the observed galaxies (number magnitude, size magnitude, ellipticity, and redshift distributions) as found in recent deep redshift and angular size surveys (Schade et al. 1995; Mutz et al. 1994). The redshift distribution we use is similar to that derived from four-color photometry of the HDF (Mobasher et al. 1996), although lacking a distinct peak at $z \sim 2$.

The lens distortions for galaxies in each redshift shell are computed using the galaxies in all of the shells in front of it. After the cumulative distortions for all redshift shells are calculated, the image is convolved with the PSF, binned down to the CCD resolution, and HDF-derived photon and readout noises are added. All galaxies are modeled as soft core isothermal distributions (Grossman & Narayan 1988) but with an outer mass cutoff, giving for the spherical case a surface density distribution outside the core:

$$\Sigma = \Sigma_o(\beta/2r)(1 + r^2/r_{\rm outer}^2)^{-1}, \quad (1)$$

where $\Sigma_o = \sigma_v^2/2G$, σ_σ is the line-of-sight velocity dispersion, $r_{\rm outer}$ is the outer mass cutoff, and $\beta = (1 + r_{\rm core}^2/r_{\rm outer}^2)$. For the candidate background galaxies, we measure the image distortion in terms of the (r, θ) second moments i_{rr} and $i_{\theta\theta}$:

$$T(r) = \frac{i_{\theta\theta} - i_{rr}}{i_{\theta\theta} + i_{rr}} = \frac{2\gamma(r)[1 - \kappa(r)]}{[1 - \kappa(r)^2 + \gamma^2(r)}, \quad (2)$$

where the convergence $\kappa(r) = \Sigma(r)/\Sigma_c$ and the shear $\gamma(r) = [\bar{\Sigma}(r) - \Sigma(r)]/\Sigma_c$ (Miralda-Escudé 1991), and where Σ_c is the critical surface mass density. We plot curves for the resulting simulated distortion $T(r)$, corrected for the cluster calibration and efficiency described below, for three values of foreground lens galaxy mass in Figure 2. All three have outer cutoff radii of 30 h^{-1} kpc, soft core radii of 1.0 h^{-1} kpc, and line-of-sight velocity dispersions as labeled.

The critical surface density is related to the distance ratio: $\Sigma_c = c^2/(4\pi GD)$. The distance ratio for a foreground-background pair is (cf. Blandford & Narayan 1992)

$$D = \frac{(1 - q_o - d_1 d_2)(d_1 - d_2)}{(1 - q_o - d_2)(1 - d_2)(1 + z_{fg})}, \quad (3)$$

where $d_1 = (1 + q_o z_{fg})^{1/2}$ and $d_2 = (1 + q_o z_{bg})^{1/2}$. By averaging over many different galaxies we are averaging D over the distributions of z_{fg} and z_{bg}. We combine these uncertainties, including multiple scattering and the FOCAS arclet detection efficiency, in a single "efficiency function" $Q(r)$. In the weak lensing regime,

$$Q = \frac{T_{\rm obs}}{T_{\rm calc}(D = 1)}, \quad (4)$$

where $T_{\rm calc}(D = 1)$ is the analytic expection of the distortion for $D = 1$. The value of $Q(r)$ is determined by comparing the prediction for single galaxy-galaxy lensing from equation (2) with the results of the three-dimensional simulations of the HDF galaxy-galaxy lensing, including multiple scattering, normalizing to the galaxy cluster data. In this way, we construct an absolute calibration for the distortion-σ_v relation. A total of 4368 CPU hours of time on an SGI Power Challenger were needed to perform the simulations. Figure 3 shows a plot of Q versus r. Over the radial range of our data a constant $Q = 0.33$ is a good overall approximation.

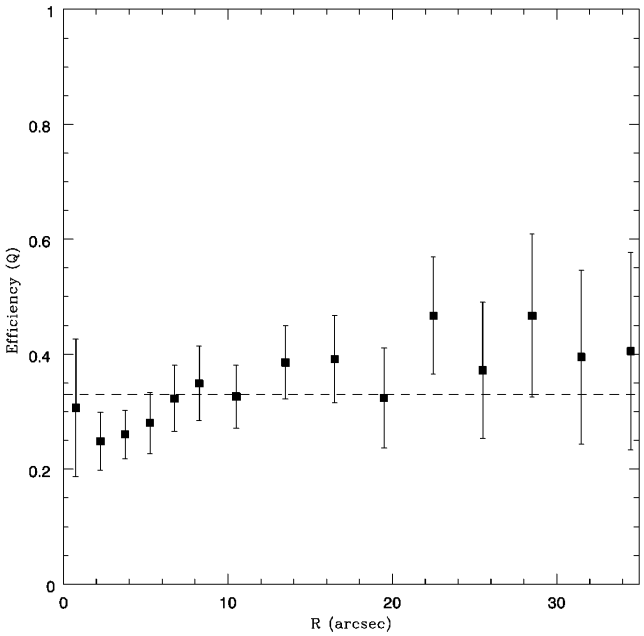

FIG. 3.—Product of distance ratio and efficiency for recovery of the distortion as a function of radius from the foreground galaxy, from the simulations. Q includes the effects of source and lens redshifts and is calibrated by normalizing $Q_{\rm sim}/Q_{\rm obs}$ to a lens of known mass, CL 0024+1654. The 1 σ error bars are derived from the scatter in measured distortion in the simulations. The dashed line is the value of Q used in plotting the curves in Fig. 2.

If we have used the correct redshift distributions, etc., in our simulations, this procedure should give reliable distortion predictions. We can largely eliminate such redshift uncertainties by simulating a lens of known mass. To fix the mass zero point for the simulation-based mass calibration we cross calibrate to a deep *HST* image of a massive cluster of galaxies at $z = 0.4$. The same three-dimensional simulation is run for CL 0024+1654 and compared with the observed weak lensing signal in the *HST* WFPC2 image of this cluster, using identical arclet selection rules. We find a similar (but 10% lower) efficiency for distortion measurement in the cluster data at a radius where the mean distortion is equal to the HDF signal at 2″. The curves plotted in Figure 2 have these calibration corrections applied.

3.2. *Systematics*

A minor correction is made for the field distortion and the spatial variation of the WFPC2 PSF by using star-dominated WFPC2 images of the LMC. Corrections due to the drizzle algorithm were found to be quite small: measurement of the signal using undrizzled data yielded statistically indistinguishable results. Other systematic errors which would be present in the HDF data, via photometry or sample selection or shear analysis, are present also in the full simulations. Therefore, by comparing observed distortion in the PSF-corrected data and simulations, the derived limits on lens mass are not biased by systematics. One sanity check is to reverse the pairs: use arclets as lenses and lenses as arclets. This gives a zero distortion (0.006 ± 0.019). Another check is to scramble the coordinates

of arclets in the catalog and recalculate the distortion: again null (0.009 ± 0.02). Similarly, scrambling the positions of the foreground galaxies yields a zero signal (0.01 ± 0.02). Finally, each of the three WFPC2 chips independently shows positive shear within 2″ in the HDF. As a check on the FOCAS software, we measured the distortion signal from a set of simulations identical to the ones used for calibration but with the lensing turned off. This resulted in a null signal (1.2 σ negative in the innermost bin).

However, spiral arms in foreground galaxies in the HDF might occasionally be split off by FOCAS and mistaken for arcs. The simulations include the ellipticity distribution of bright galaxies but not spiral arms. To check this, we take wider field deep ground-based imaging (0.″5 pixels) and run FOCAS with the same parameters as with the HDF data, calling each pixel 0.″04 and scaling the magnitudes accordingly. This generates 38,900 pairs of galaxies with scaled apparent magnitudes and angular sizes similar to the HDF. We obtain a null result for the observed distortion in this surrogate data: at 2″ radius (25″ in the original wide-field data) we find a mean distortion of 0.0011 ± 0.0016, and at 1″ we find 0.0019 ± 0.0025. Thus, spiral arms are apparently not a source of systematic error in the HDF shear measurements, down to 1″ radius, on the scale of our observed distortion.

4. AVERAGE GALAXY MASS

Using $Q(r)$, the product of efficiency and average distance ratio, from the cluster-calibrated three-dimensional simulations to normalize the analytic expression in equation (1) to the HDF distortion data, we find a best-fit galaxy velocity dispersion σ_v of 185^{+30}_{-35} km s^{-1} for outer truncation radii larger than 15 h^{-1} kpc and $r_{\rm core} \leq 2\ h^{-1}$ kpc. This corresponds to a distortion at 2″ of $0.066^{+0.018}_{-0.019}$. The average mass interior to 20 h^{-1} kpc is $5.9^{+2.5}_{-2.7} \times 10^{11}\ h^{-1}\ M_\odot$. For $\sigma_v = 185$ km s^{-1}, the core radius is $r_{\rm core} = 0.6^{+1.3}_{-0.6}\ h^{-1}$ kpc. From the absence of an odd image in strongly lensed QSOs, Wallington & Narayan (1993) argue for mass cores less than 200 pc. The HDF data are consistent with this requirement, although our upper limits are not as stringent.

Fixing σ_v at 185 km s^{-1}, we find an acceptable fit for truncation radii $r_{\rm outer} > 3.''5$ ($>15\,h^{-1}$ kpc). Inside $\approx 10\,h^{-1}$ kpc, the rest-frame V band mass-to-light ratio is $11.4^{+6.0}_{-6.7}\ h\ (M/L_V)_\odot$. VLA-based lensed QSO data sample smaller galaxy radii and find correspondingly smaller M/L (see Fassnacht et al. 1996). Our M/L for the whole field galaxy population suggests a halo increasingly dominated by dark matter beyond $10\ h^{-1}$ kpc. In this Letter we have only examined isothermal models. The radial profiles of our observed and calculated shear are different; we will explore this at greater length elsewhere, combining various deep *HST* and ground-based data.

We briefly compare our results with the recent observations of galaxy-galaxy lensing by Brainerd et al. (1996). Although both studies probe galaxy-galaxy lensing, they do so on different scales. The Brainerd et al. observations sample a region outside 5″ or $\sim 15 h^{-1}$ kpc for their sample. By contrast, our sample shows strong distortion precisely inside this region. Extrapolating their distortion at 10″ to smaller radii yields a somewhat greater signal than is seen in the HDF. Ultimately, the distribution of galaxy mass on these larger scales will be addressed by comparably deep surveys covering hundreds of times the area of the HDF. In particular, these surveys will have to go significantly deeper than the "Groth Strip" which covers 144 arcmin^2, imaged with the *HST* in two filters: F555W and F814W. This covers 27 times the area of the HDF, but 3 mag shallower, resulting in fewer close pairs. Because the candidate arclets are brighter and hence lower redshift, the lensing efficiency is also reduced. For the Groth strip, we find a distortion 0.015 ± 0.009 for 492 foreground-background pairs within 5″, roughly consistent with the HDF results, although with much greater uncertainty.

We gratefully acknowledge the help of Tom Duff, Greg Kochanski, Rick Wenk, discussions with Andy Fruchter, Allen Mills, Penny Sackett, and Peter Schneider, suggestions of the referee. Peter Schneider, Phil Fischer kindly supplied the WFPC2 LMC data. We thank Bob Williams and the HDF team at STScI for rapidly making these data available to the community.

REFERENCES

Blandford, R. D., & Narayan, R. 1992, ARA&A, 30, 311
Brainerd, T. G., Blandford, R. D., & Smail, I. 1996, ApJ, 466, 623
Fassnacht, C. D., et al. 1996, ApJ, 460, L103
Fich, M., & Tremaine, S. D. 1991, ARA&A, 29, 409
Grossman, S. A., & Narayan, R. 1988, ApJ, 324, L37
Im, M., Casertano, S., Griffiths, R. E., Ratnatunga, K. U., & Tyson, J. A. 1995, ApJ, 441, 494
Kochanek, C. S. 1991 ApJ, 373, 354
Koo, D., & Kron, R. 1992, ARA&A, 30, 613
Lilly, S. J., Tresse L., Hammer, F., Crampton D., & Le Fevre, O. 1995, ApJ, 455, 108
Miralda-Escudé, J. 1991, ApJ, 370, 1
Mobasher, B., Rowan-Robinson, M., Georgakakis, A., & Eaton, N. 1996, preprint SISSA/astro-ph9604118
Mutz, S. B., et al. 1994, ApJ 434, L55
Schade, D., Lilly, S. J., Crampton, D., Hammer, F., Le Fevre, O., & Tresse, L. 1995, ApJ, 451, L1
Tyson, J. A. 1987, in Theory and Observational Limits in Cosmology, ed. W. R. Stoeger (Rome: Specola Vaticana), 441
Tyson, J. A., Valdes, F., Jarvis, J. F., & Mills, A. P. 1984, ApJ, 281, L59
Tyson, J. A., Valdes, F., & Wenk, R. A. 1990, ApJ, 349, L1
Wallington, S., & Narayan, R. 1993, ApJ, 403, 517
Williams, R., et al. 1996, in Science with the *Hubble Space Telescope*, Vol. 2, ed. P. Benvenuti, F. D. Maccetto, & E. J. Schreier (Baltimore: STScI), 1996
Zaritsky, D., & White, S. D. M. 1994, ApJ, 435, 599